

MODELING REACTION KINETICS OF ZNO MICROPARTICLES SYNTHESIZED VIA MICROWAVE: AB INITIO SIMULATION

Mendoza-Báez R., Morales M.A., Luna-Flores A., Agustin-Serrano R., Cervantes-Tavera A.M., Hernandez-Santiago A.A.

Meritorious Autonomous University of Puebla

Puebla, Mexico

Received: 20.07.2020

Abstract. The nucleation and growth mechanisms of nanoparticles and micro-particles of semiconductor materials has not been fully disclosed and for sure. Therefore, a theoretical and experimental experiment is proposed to investigate in a first stage the nucleation mechanism through the reaction mechanism. Zinc oxide micro-particles were synthesized from zinc acetate dihydrate and sodium hydroxide in the presence of ethanol in aqueous medium, via a microwave-assisted hydrothermal method. The subjacent molecular mechanism of the experimental process was researched by *ab initio* calculations with the 3-21G basis set. We found that the microwave radiation system is crucial during the synthesis for the nucleation mechanism of zinc oxide microparticles, since it provides the necessary energy to carry out the endothermic reaction where the $Zn(OH)_4^{2-}$ complex is produced, which in turn, through an exothermic and spontaneous reaction for the obtaining of zinc oxide (ZnO) as product of the reaction mechanism. SEM micrographs of the resulting microparticles show that ZnO has a branched morphology and the XRD pattern exhibit a crystal size to nanometric scale (31.3 nm). Both theoretical and experimental results support the kinetics of the proposed reaction mechanism.

Key words: Reaction-mechanism, dioxide zinc, microwaves, AB INITIO, branched morphology.

INTRODUCTION

New micro and nanostructured materials based on metals and metal oxides are currently under investigation due to their wide applications such as photo-catalytic degradation [1, 2], antibacterial compounds [3] and solar energy [4]. Thus, many investigations have focused on knowing the critical variables on which the conformation of a certain morphology depends, for example, micro and nanoparticles in the form of tubes, wires, flowers, stars, discs, clusters, leaves, needles, boxes, walnuts, cubes [5, 6], among other geometries. For example, branched nanostructures such as silver phosphate have an improved photocatalytic activity, compared to the geometric structures mentioned above. [7].

In particular, zinc oxide is an important material because it possesses excellent optical, electrical and microstructural properties [8-10], making it a good candidate for applications in visible and ultraviolet light emitters, transparent field-effect transistors, photodetectors, solar cells, sensors and piezoelectric devices [11-14]. There are different synthesis methods to obtain ZnO nanostructures such as the sol-gel method, spray pyrolysis, liquid combustion reaction, hydrothermal synthesis, chemical vapor deposition (CVD), the Pechini method [15-19] and, currently, bio-mediated synthesis [20]. Many researchers have employed *ab initio* methods to study the electronic and structural properties of different ZnO structures, however, it is always at the unit cell level or crystal structure level [21-23]. In this research work, *ab initio* calculations were performed to theoretically confirm the proposed reaction kinetics based on experimental synthesis assisted by microwave, considering zinc oxide as a product of reaction kinetics. The reaction mechanism obtained provides an explanation of the nucleation mechanism. This work is the basis for future studies on multiscale modeling of nucleation and growth of branched (fractal) structures.

MATERIALS AND METHODS

The synthesis of zinc oxide microparticles (ZnOMPs) was carried out using zinc acetate dihydrate ($Zn(CH_3COO)_2 \cdot 2(H_2O)$) ≥99% purity (J.T.Baker) and sodium hydroxide (NaOH) ≥98% (J.T.Baker) as precursor and catalyst, respectively. Furthermore, to carry out the synthesis, methanol (CH_3OH) ≥99% (Sigma-Aldrich) was used as reagent and distilled water as solvent. The zinc oxide microstructures were synthesized using the microwave assisted hydrothermal method. First, a 0.2 M solution of zinc acetate dihydrate in methanol (Sol1) was prepared, which was subjected to mechanical stirring for ~ 10 min. Then, another 1.0 M solution (Sol2) of sodium hydroxide in distilled water was prepared. Without stopping the stirring of Sol1, Sol2 is added and the stirring is continued for 60 minutes. After the stirring time of the Sol1-Sol2 mixture, it is subjected to microwave radiation for 10 minutes at 50% of the equipment power (Fig. 1). Finally, the resulting solution is centrifuged at 300 rpm for 10 minutes, obtaining two phases: a liquid phase at the top and the solid phase of the synthesized ZnO deposited at the bottom of the centrifuge tube. The microwave radiation equipment is a modified conventional microwave from the brand Daewoo model KOR-662M.

1.1 Computational Details.

To theoretically evaluate the thermodynamic parameters of all the chemical species involved in the reaction mechanism, all structures were optimized with Hartree-Fock methods, using the 3-21G basis set [24,25] implemented in the package of Gaussian program 09 [26]. Using the conductor-like polarizable continuum model (CPCM) [27,28], the

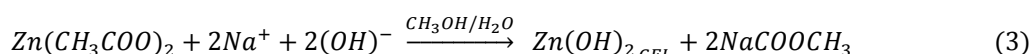


Figure 1. Microwave radiation system with arrangement of the Sol1-Sol2 mixture and cooling system on top of equipment

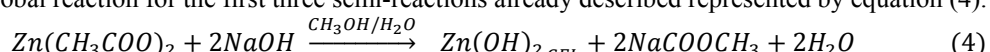
total energies of the molecules of reagents, products and transition states in solvent water and methanol were calculated, since all reactions occur in the presence of these two species from the dissociation of the precursors to the final product. For each of the half-reactions, the Gibbs free energy ($\Delta_r G^\circ$) and the reaction enthalpy ($\Delta_r H^\circ$) were obtained. Frequency calculations were performed at the same theoretical level (HF 3-21G / CPCM) to check the nature of stationary points on the potential energy surface (PES), obtaining no imaginary frequencies for both reagent molecules and transition states. Recent studies maintain the same level of theory for geometric optimizations and for frequency calculations [29-31]. In addition, the frequency calculations obtained the thermodynamic parameters zero-point energy (ZPE), thermal contributions to enthalpy (ΔH), Gibbs free energy (ΔG) and entropy (ΔS), at a temperature equal to 298 K. Data analysis was done using GaussView 6.0 (Gaussian, Inc.).

1.2 Reaction Mechanism.

The synthesis process of ZnOMPs begins with the preparation of Sol1 and Sol2 corresponding to the dehydration of $Zn(CH_3COO)_2 \cdot 2(H_2O)$ and the dissociation of NaOH, respectively, as shown in equations (1) and (2) (Figure 2). Zinc acetate dihydrate fails to fully dissociate into Zn^{2+} and $(OH)^-$ because methanol is not polar enough, unlike water. Then, when mixing both solutions (Sol1-Sol2), the dissociation of zinc acetate occurs by reaction with the Na^+ and $(OH)^-$ ions previously dissociated in Sol2, as shown in equation (3) (Figure 3), obtaining as zinc hydroxide product ($Zn(OH)_2$) and sodium acetate ($NaCOOCH_3$). Bari *et al.* [32] describe that zinc hydroxide acetate is an intermediate of the hydrolysis reaction, formed in the presence of H_2O molecules and ions $(OH)^-$, which can be easily transformed into ZnO at higher temperatures and with prolonged reflux, while sodium acetate is soluble in water and could therefore be removed from the final product. Yung *et al.* [33] mention that the abundance of electrons in the oxygen atoms causes the hydroxyl (OH) groups of the alcohol molecules to bind with the zinc ions. On the other hand, Haase *et al.* [34] also reported that it is favorable to use alcohol as a solvent, since it helps react the Zn^{2+} ions and NaOH, due to the dehydrating property of the alcohol, preventing the formation of zinc hydroxide.



Therefore, there is a global reaction for the first three semi-reactions already described represented by equation (4).



The precipitation mechanism proposed by Wu *et al.* [35] explains that $Zn(CH_3COO)_2$ can be converted to colloidal $Zn(OH)_2$ under an alkaline solution with a pH value between 13 and 14. Usually, in a synthesis using the sol-gel technique, there is a hydrothermal process where part of the colloids $Zn(OH)_2$ dissolves in Zn^{2+} and $(OH)^-$ as shown in equation (5) (Figure 4.a). Then, an anionic complex of zinc coordinate to four hydroxyl radicals ($Zn(OH)_4^{2-}$) is formed, denoted in

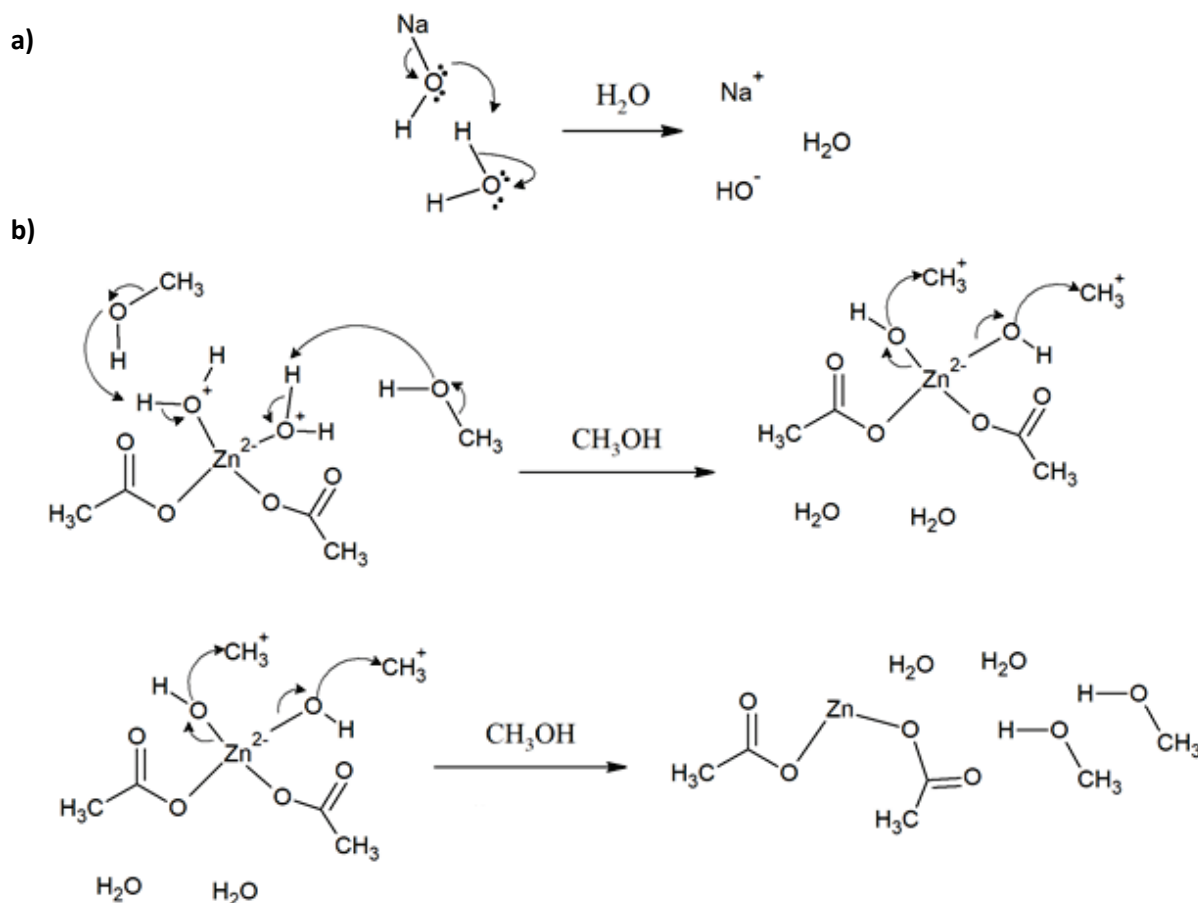


Figure 2. Reaction mechanisms proposed for a) dissociation of NaOH in aqueous medium and b) dehydration of $Zn(CH_3COO)_2 \cdot 2(H_2O)$ in methanol

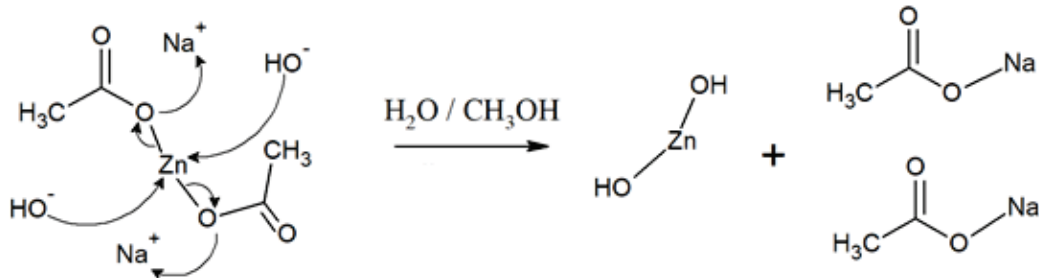
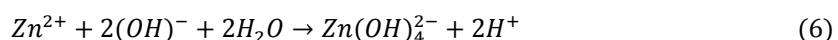
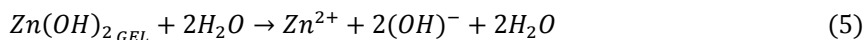
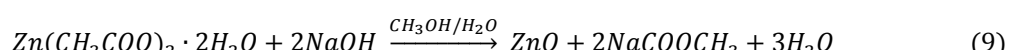
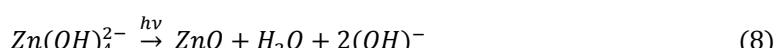
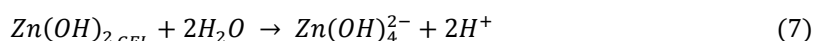


Figure 3. Reaction mechanism in the Sol1-Sol2 mixture, production of $Zn(OH)_2$

equation (6) (Figure 4.b). When the concentration of Zn^{2+} and $(OH)^-$ reaches the degree of ZnO supersaturation, ZnO nuclei will be formed according to the reaction of equation (8), going through an intermediate complex proposed by Smith *et al.* [36] called oxodihydroxyzincate, $ZnO(OH)_2^{2-}$ (Figure 4.c). Finally, adding all the semi-reactions in a global reaction, equation (9) is obtained.



Equation (7) is the sum of half-reactions (5) and (6):



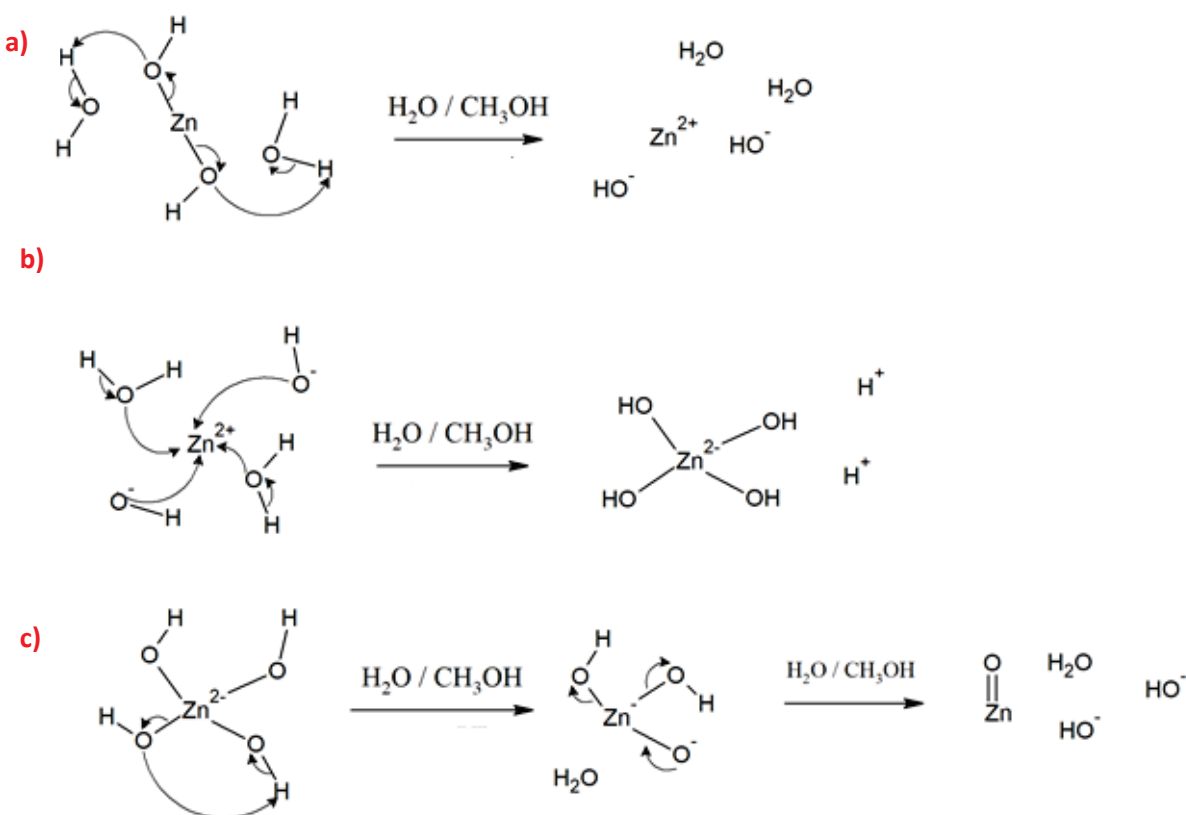


Figure 4. Reaction mechanisms of a) dissociation of zinc hydroxide, b) formation of the coordinated zinc anion complex, and c) obtaining ZnO

Wu *et al.* show that the temperature at which the hydrothermal process is carried out in the synthesis of ZnO nanoparticles (ZnONPs) is essential to obtain different nanostructures, for example, at 70°C, rod-shaped nanoparticles are obtained, while at 90°C prismatic nanostructures are obtained. Furthermore, experiments carried out by Aquino *et al.* [37] show that by performing the synthesis at 50°C, ZnONPs with a wurtzite-like structure are produced. In this work, the thermal energy that the hydrothermal process provides to terminal chemical reactions was provided by microwave radiation.

RESULTS AND DISCUSSION

Table 1 summarizes the thermochemical values obtained for each of the chemical species involved in the complete reaction mechanism, under the HF 3-21G / CPCM quantum chemical level of theory. These values are necessary to calculate the enthalpy of reaction and Gibbs free energy of reaction of each semi-reaction involved, shown in Table 2.

From the values shown in Table 2, it is observed that the reactions of equations (1)-(3) and (8) are spontaneous and exothermic processes since the Gibbs free energy values of reaction and enthalpy of reaction are negative, while on the other hand, the reactions of equations (5) and (6) show a positive value in $\Delta_r G^\circ$ and $\Delta_r H^\circ$ indicating endothermic and not spontaneous reactions. These results are consistent with the synthesis process, since just in non-spontaneous endothermic reactions [Eq. (5) and (6)] correspond to the microwave radiation process, that is, it provides the necessary thermal energy to carry out the dissociation of the precipitated gel Zn(OH)₂ to form the Zn(OH)₄²⁻ complex. Then, the power configured in the microwave radiation equipment (Fig. 1) is crucial to form the ZnO Ps, if the energy supplied to the system is not enough, it will be obtained as the product Zn(OH)₂.

Calculations of the band gap energy between the highest orbital molecular occupied (HOMO) and the lowest unoccupied molecular orbital (LUMO, Eg), and quantum molecular descriptors such as chemical potential (μ), global hardness (η) and the electrophilicity index (ω) were obtained to study the chemical reactivity and stability of the molecules involved [38]. The quantum molecular descriptors are determined from the values of the energies of the HOMO and LUMO, by means of the equations established in the Koopman's theorem [39]. Therefore, μ and η can be calculated with equations (10) and (11), respectively:

$$\mu = \left(\frac{\partial E}{\partial N} \right)_{v(r)} = -\frac{I + A}{2}, \quad (10)$$

$$\eta = \left(\frac{\partial^2 E}{\partial N^2} \right)_{v(r)} = \frac{I - A}{2}, \quad (11)$$

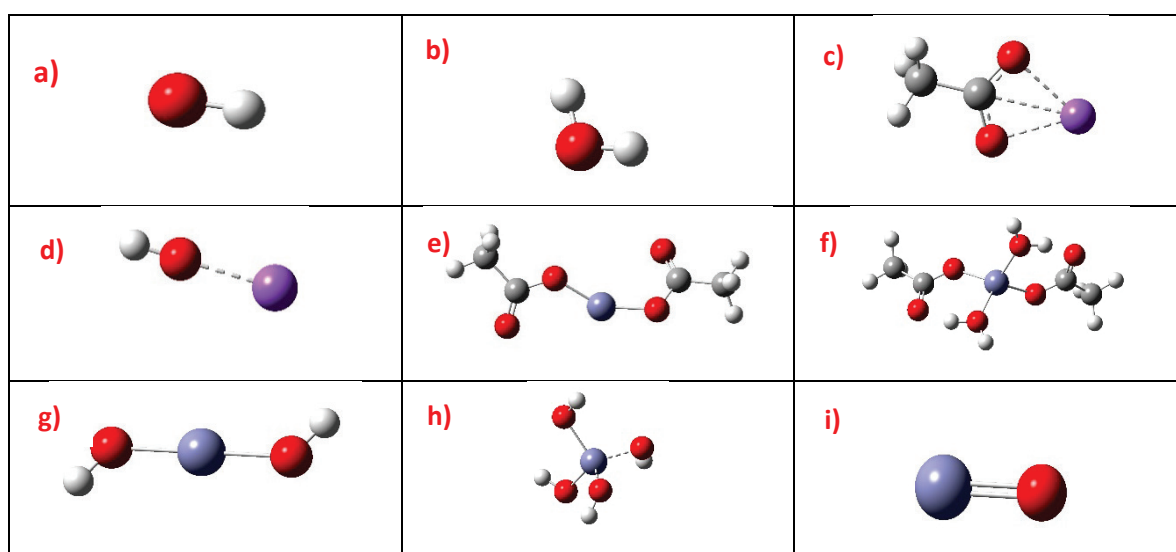


Figure 5. Optimized molecular structures: a) hydroxyl ion; b) water; c) sodium acetate; d) sodium hydroxide; e) zinc acetate; f) zinc acetate dihydrate; g) zinc hydroxide; h) zinc tetrahydroxide complex; i) molecular ZnO

where $I = -E_{HOMO}$ is the ionization potential, $A = -E_{LUMO}$, I/A is the electronic affinity, E is the total energy, N is the number of electrons and $v(r)$ is the external potential of the system [40]. The global electrophilicity index is described by Parr [41], employs the electronic chemical potential and is given by:

$$\omega = \frac{\mu^2}{2\eta}.$$

This descriptor measures the tendency of chemical species to accept electrons. Small values of ω indicate that the chemical species behaves like an electron donor (nucleophile), while high values of ω characterize a chemical species that behaves as an electron acceptor (electrophile).

Time-Dependent Density Functional Theory (TD-DFT) has become the most widely-used theoretical approach to simulate the optical properties of both organic and inorganic molecules [42]. Since the final product (ZnO Ps) has important optical properties, the energy of the zinc oxide molecule with TD-DFT was calculated with the 3-21G basis set, replacing the Hartree-Fock / 3-21G calculations. Table 3 summarizes the values obtained from the quantum molecular descriptors, as well as the HOMO-LUMO gap, noting that for ZnO a value very close to the experimental one [43] is obtained.

The ZnO Ps obtained by microwave-assisted hydrothermal synthesis were characterized by SEM, finding that they possess a branched structure of micrometrical size (Fig. 7). Furthermore, X-ray diffraction (XRD) shows the crystalline phase of the microparticles (Fig. 8) with crystal size of 31.3 nm. The diffraction pattern corresponds to Wurtzite-type hexagonal ZnO with lattice parameters $a = b = 3.253$ and $c = 5.213$ Å.

Table 1. Thermochemical values calculated in (kJ/mol) for the reagents, intermediates and products in the synthesis of ZnO MPs

Chemical Compound	Electronic Energy (E_0)	$E_0 + H_{corr}$	$E_0 + G_{corr}$
Zn(CH ₃ COO) ₂ .2H ₂ O	-6229100.196	-6228671.972	-6228831.069
Zn(CH ₃ COO) ₂	-5831899.558	-5831609.952	-5831752.874
H ₂ O	-199610.3241	-199547.7112	-199603.7656
NaOH	-623048.2527	-623007.2792	-623074.2215
Na ⁺	-424867.9283	-424861.7321	-424905.8116
(OH) ⁻	-198280.7761	-198251.3206	-198302.6255
Zn(OH) ₂	-5063750.81	-5063674.505	-5063761.572
NaC ₂ O ₄	-1015871.665	-1015727.325	-1015828.121
Zn ²⁺	-4666760.217	-4666754.021	-4666801.902
Zn(OH) ₄ ²⁻	-5433561.054	-5433418.011	-5433535.907
H ⁺	-424.2283223	-418.0321418	-450.4833243
ZnO	-4840262.137	-4840248.621	-4840315.219

Table 2. Enthalpy and Gibbs free energy (kJ/mol) of reaction for each half-reaction

Equation Number	(1)	(2)	(3)	(5)	(6)	(8)
$\Delta_r H^\circ$	-2033.402645	-211.5470531	-17293.09861	417.843106	28098.00862	-2880.961369
$\Delta_r G^\circ$	-2129.335797	-268.4311404	-17248.06603	354.418897	28177.8107	-2988.328575

Table 3. Quantum Molecular Descriptors of molecules (eV)

Descriptors	Zn(CH ₃ COO) ₂	NaOH	Zn(OH) ₂	Zn ²⁺	Zn(OH) ₄ ²⁻	ZnO
E_{TOTAL}	-60443.39505	-6457.44175	-52482.0923	-48367.5737	-56314.9063	-50217.5126
E_{HOMO}	-11.0929989	-9.13513876	-11.8072981	-22.0474918	9.9215482	-4.83628194
E_{LUMO}	2.5907973	-0.28191009	0.6944349	-2.92957922	26.08267	-1.32628359
$E_g (HOMO-LUMO)$	13.6837962	8.85322867	12.501733	19.1179126	16.1611218	3.50999835
$I = -E_{HOMO}$	11.0929989	9.13513876	11.8072981	22.0474918	-9.9215482	4.83628194
$A = -E_{LUMO}$	-2.5907973	0.28191009	-0.6944349	2.92957922	-26.08267	1.32628359
$\eta = (I - A)/2$	6.8418981	4.42661433	6.2508665	9.55895629	8.0805609	1.75499918
$\mu = -(I + A)/2$	-4.2511008	-4.70852443	-5.5564316	-12.4885355	18.0021091	-3.08128277
$\omega = \mu^2/2\eta$	1.320675765	2.50419402	2.46957219	8.15797847	20.0528117	2.70493104

CONCLUSIONS

In this work, ab initio calculations with Hartree-Fock methods and 3-21G basis set were implemented to study the reaction kinetics in the synthesis of ZnO microparticles by microwave-assisted hydrothermal method. The theoretical part shows the thermochemical parameters of the chemical reactions that are carried out, as well as the reactivity of the molecules involved in the entire synthesis process, confirming which chemical reactions are thermodynamically favorable.

On the other hand, the experimental part shows that the ZnO MPs have a branched morphology with nanometric crystal size and that the microwave-assisted hydrothermal method is an economical, easy to make and efficient method for obtaining ZnO microparticles. It implies that the results obtained so far, will serve as the basis for further detailed research on the nucleation and growth of ZnO microparticles with branched morphology.

Therefore, the following hypotheses can be formulated: the synthesis process of ZnO MPs with branched morphology have underlying processes concatenated in series at three different scales such as molecular, nanometric and micrometric. The reaction mechanism describes completely the molecular process with AB INITIO simulation, while that the micrometrical growth process could be explained by model of crystal phase field that reveal the mechanism of tridimensional dendritic solidification [1]. The mesoscale process (nanometric) could be given by a reaction-diffusion system with the ability of unified the molecular and nanometric scales, that serve as base of the nucleation mechanism by means of an auto-ensemble or/and auto-organization processes.

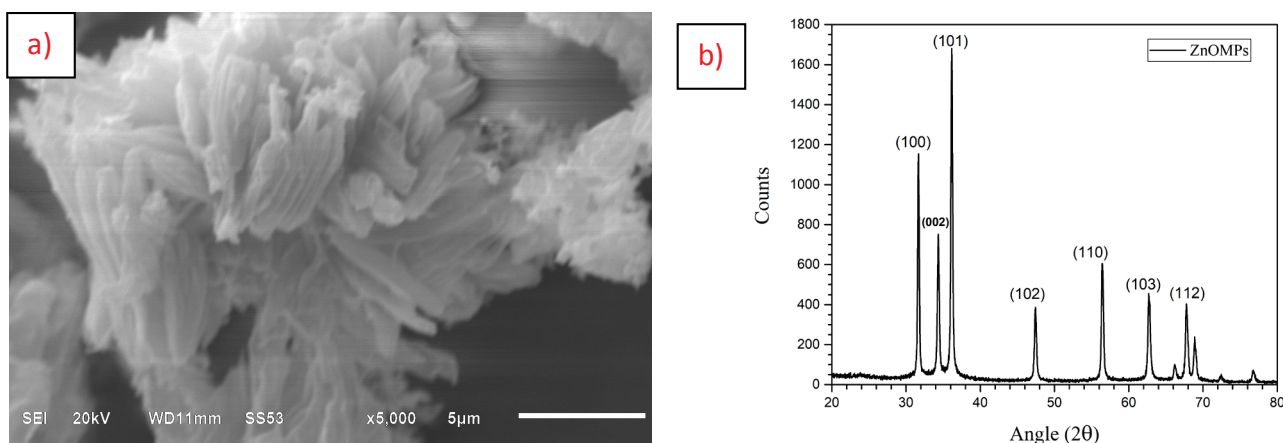


Figure 7. a) SEM micrograph of the morphology of ZnO microparticles and b) X-ray diffraction pattern of ZnOMPs synthesized by microwave-assisted hydrothermal method

References:

1. Morales M.A., Fernández-Cervantes I., Agustín-Serrano R., Ruiz-Salgado S., Sampedro M.P., Varela-Caselis J.L., Rubio E. Ag_3PO_4 microcrystals with complex polyhedral morphologies diversity obtained by microwave-hydrothermal synthesis for MB degradation under sunlight. *Results in Physics*, 2019, vol. 12, pp. 1344-1356. DOI: 10.1016/j.rinp.2018.12.082.
2. Wang J., Lee Y.-J., Hsu J.W.P. One-step synthesis of ZnO Nanocrystals in n-butanol with bandgap control: applications in hybrid and organic photovoltaic devices. *J Phys Chem C*, 2014, vol. 118, pp. 18417-18423.
3. Nair S., Sasidharan A., Divya Rani V.V., Menon D., Nair S., Manzoor K., Raina S. Role of size scale of ZnO nanoparticles and microparticles on toxicity toward bacteria and osteoblast cancer cells. *Journal of Materials Science: Materials in Medicine*, 2008, vol. 20 (S1), pp. 235-241. DOI: 10.1007/s10856-008-3548-5.
4. McCune M., Zhang W., Deng Y. High efficiency dyesensitized solar cells based on three-dimensional multilayered ZnO nanowire arrays with “caterpillar-like” structure. *Nano Lett*, 2012, vol. 12, pp. 3656-3662.
5. Rycenga M., Cobley C.M., Zeng J., Li W., Moran C.H., Zhang Q., Xia Y. Controlling the Synthesis and Assembly of Silver Nanostructures for Plasmonic Applications. *Chemical Reviews*, 2011, vol. 111(6), pp. 3669-3712. DOI: 10.1021/cr100275d.
6. Sun Y. Shape-Controlled Synthesis of Gold and Silver Nanoparticles. *Science*, 2002, vol. 298 (5601), pp. 2176-2179. DOI: 10.1126/science.1077229.
7. Batvandi M., Haghightzadeh A., Mazinani B. Synthesis of Ag_3PO_4 microstructures with morphology-dependent optical and photocatalytic behaviors. *Applied Physics A*, 2020, vol. 126 (7). DOI: 10.1007/s00339-020-03761-6.
8. Klingshirn C.F., Meyer B.K., Waag A., Axel H., Johannes M.M. Zinc Oxide: From Fundamental Properties Towards Novel Applications. *Springer*, 2010, pp. 9-10. ISBN 978-3-642-10576-0.
9. Baruah S., Dutta J., Dutta «Hydrothermal growth of ZnO nanostructures». *Sci. Technol. Adv. Mater.*, (free download) 2009, vol. 10, p. 013001. Bibcode: 2009STAdM..10a3001B. DOI: 10.1088/1468-6996/10/1/013001.
10. Özgür Ü., Alivov Ya.I., Liu C., Teke A., Reshchikov M.A., Doğan S., Avrutin V., Cho S.-J. et al. A comprehensive review of ZnO materials and devices. *Journal of Applied Physics*, 2005, vol. 98 (4), p. 041301. Bibcode: 2005JAP....98d1301O. DOI: 10.1063/1.1992666.
11. Hamdani F., Botchkarev A., Kim W., Morkoc H., Yeadow M., Gibson J.M., Tsen S.C.Y., Smith D.J., Evans K., Litton C.W., Michel W.C., Hemenger P. *Appl. Phys. Lett.*, 1997, vol. 70, p. 467.
12. Nomura K., Ohta H., Ueda K., Kamiya T., Hirano M., Hosono H. *Science*, 2003, vol. 300, p. 1269.
13. Huang M.H., Mao S., Feick H., Yan H., Wu Y., Kind H., Weber E., Russo R., Yang P. *Science*, 2001, vol. 292, p. 1897.
14. Lee C.T., Su Y.K., Wang H.M. *Thin Solid Films*, 1987, vol. 150, p. 283.
15. Silva R.F. Filmes de óxido de zinco dopado com alumínio ou európio: Preparação e caracterização. Tese (Doutorado), Faculdade de Filosofia. *Ciências e Letras de Ribeirão Preto*, 2001.
16. Abrarov S.M., Yuldashev Sh.U., Lee S.B., Kang T.W. Suppression of the green photoluminescence band in ZnO embedded into porous opal by spray pyrolysis. *Journal of Luminescence*, 2004, vol. 109, pp. 25-29.
17. Sousa V.C. et al. Combustion synthesized ZnO powders for varistor ceramics. *International Journal of Inorganic Materials*, 1999, vol. 1, pp. 235-241.
18. Wang J., Gao L. Hydrothermal synthesis and photoluminescence properties of ZnO nanowires. *Solid State Communications*, 2004, vol. 132, pp. 269-271.
19. Lima S.A.M., Sigoli F.A., Davolos M.R., Jafelicci Jr.M. Europium (III)-containing zinc oxide from Pechini method. *Journal of Alloys and Compounds*, 2002, vol. 344, pp. 280-284.
20. Sharma D., Sabela M.I., Kanchi S., Bisetty K., Skelton A.A., Honarpourvar B. Green synthesis, characterization and electrochemical sensing of silymarin by ZnO nanoparticles: Experimental and DFT studies. *Journal of Electroanalytical Chemistry*, 2018, vol. 808, pp. 160-172. DOI: 10.1016/j.jelechem.2017.11.039.
21. Sun J., Wang H.-T., He J., Tian Y. Ab initio investigations of optical properties of the high-pressure phases of ZnO. *Physical Review B*, 2005, vol. 71 (12). DOI: 10.1103/physrevb.71.125132.
22. Serrano J., Romero A.H., Manjón F.J., Lauck R., Cardona M., Rubio A. Pressure dependence of the lattice dynamics of ZnO: An ab initio approach. *Physical Review B*, 2004, vol. 69 (9). DOI: 10.1103/physrevb.69.094306.
23. Saib S., Bouarissa N. Structural parameters and transition pressures of ZnO: ab-initio calculations. *Physica Status Solidi (b)*, 2007, vol. 244 (3), pp. 1063-1069. DOI: 10.1002/pssb.200642441.
24. Binkley J.S., Pople, J.A., Hehre W.J. “Self-Consistent Molecular Orbital Methods. 21. Small Split-Valence Basis Sets for First-Row Elements”. *J. Am. Chem. Soc.*, 1980, vol. 102, pp. 939-47. DOI: 10.1021/ja00523a008.
25. Pietro W.J., Franel M.M., Hehre W.J., Defrees D.J., Pople J.A., Binkley J.S. “Self-Consistent Molecular Orbital Methods. 24. Supplemented small split-valence basis-sets for 2nd-row elements”. *J. Am. Chem. Soc.*, 1982, vol. 104, pp. 5039-48. DOI: 10.1021/ja00383a007.
26. Frisch M.J. et al. *Gaussian 09, revision A.1*. Gaussian Inc., Wallingford, 2009.
27. Klamt A., Schüürmann G. COSMO: a new approach to dielectric screening in solvents with explicit expressions for the screening energy and its gradient. *J. Chem. Soc., Perkin Trans.*, 1993, vol. 2, (5), pp. 799-805. DOI: 10.1039/p29930000799.

28. Barone V., Cossi M. Quantum Calculation of Molecular Energies and Energy Gradients in Solution by a Conductor Solvent Model. *The Journal of Physical Chemistry A*, 1998, vol. 102 (11), pp. 1995-2001. DOI: 10.1021/jp9716997.
29. Liu T., Zhao L., Zhong R. DFT investigations of phosphotriesters hydrolysis in aqueous solution: a model for DNA single strand scission induced by N-nitrosoureas. *Journal of Molecular Modeling*, 2012, vol. 19 (2), pp. 647-659. DOI: 10.1007/s00894-012-1592-z.
30. Mikula H., Svatunek D., Skrinjar P., Horkel E., Hametner C., Fröhlich J. DFT study of the Lewis acid mediated synthesis of 3-acyltetramic acids. *Journal of Molecular Modeling*, 2014, vol. 20 (5). DOI: 10.1007/s00894-014-2181-0.
31. Ensuncio A.E., López J.M., Robles J. Estudio Computacional de la Cinética y Mecanismos de Reducción del Colorante Rojo Allura por Bisulfito de Sodio en Fase Acuosa. *Información Tecnológica*, 2013, vol. 24 (2), pp. 15-22. DOI: 10.4067/s0718-07642013000200003.
32. Bari A.R., Shinde M.D., Vinita D., Patil L.A. Effect of Solvents on the Particle Morphology of nanostructured ZnO. *Indian Journal of Pure & Applied Physics*, 2009, vol. 47, pp. 24-27.
33. Yung K., Ming H., Yen C., Chao H. Synthesis of 1D, 2D and 3D ZnO Polycrystalline Nanostructures Using Sol-Gel Method. *Journal of Nanotechnology*, 2012, pp. 1-8.
34. Haase M., Weller H., Henglein A. "Photochemistry and Radiation Chemistry of Colloidal Semiconductors. 23. Electron Storage on ZnO Particles and Size Quantization". *The Journal of Physical Chemistry*, 1988, vol. 92, pp. 482-487.
35. Wu C., Qiao X., Chen J., Wang H., Tan F. A novel chemical route to prepare ZnO nanoparticles. *Mater Lett.*, 2006, vol. 60 (15), pp. 1828-1832.
36. Smith G.D., Bell R., Borodin O., Jaffe R.L. A Density Functional Theory Study of the Structure and Energetics of Zincate Complexes. *The Journal of Physical Chemistry A*, 2001, vol. 105 (26), pp. 6506-6512.
37. Rev Soc Quím Perú, 2018, vol. 84 (1).
38. Gázquez J.L. Perspectives on the density functional theory of chemical reactivity. *J. Mex. Chem. Soc.*, 2008, vol. 52, pp. 3-10.
39. Koopmans T. Über die Zuordnung von Wellenfunktionen und Eigenwerten zu den einzelnen Elektronen eines Atoms. *Physica*, 1934, vol. 1, pp. 104-113. DOI: 10.1016/s0031-8914(34)90011-2.
40. Parr R.G., Donnelly R.A., Levy M., Palke W.E. Electronegativity: The density functional viewpoint. *J. Chem. Phys.*, 1978, vol. 68, pp. 3801-3807. DOI: 10.1063/1.436185.
41. Parr R.G., Szentpály L.V., Liu S. Electrophilicity index. *J. Am. Chem. Soc.*, 1999, vol. 121, pp. 1922-1924. DOI: 10.1021/ja983494x.
42. Laurent A.D., Jacquemin D. TD-DFT benchmarks: A review. *International Journal of Quantum Chemistry*, 2013, vol. 113 (17), pp. 2019-2039. DOI: 10.1002/qua.24438.
43. Srikant V., Clarke D.R. On the optical band gap of zinc oxide. *Journal of Applied Physics*, 1998, vol. 83 (10), pp. 5447-5451. DOI: 10.1063/1.367375.